



HAL
open science

Atomically Precise Prediction of 2D Self-Assembly of Weakly Bonded Nanostructures: STM Insight into Concentration-Dependent Architectures

Mohamed El Garah, Arezoo Dianat, Andrea Cadeddu, Rafael Gutierrez, Marco Cecchini, Timothy R. Cook, Artur Ciesielski, Peter J. Stang, Gianaurelio Cuniberti, Paolo Samorì

► To cite this version:

Mohamed El Garah, Arezoo Dianat, Andrea Cadeddu, Rafael Gutierrez, Marco Cecchini, et al.. Atomically Precise Prediction of 2D Self-Assembly of Weakly Bonded Nanostructures: STM Insight into Concentration-Dependent Architectures. *Small*, 2016, 12 (3), pp.343-350. <10.1002/smll.201502957>. <hal-03630293>

HAL Id: hal-03630293

<https://hal.science/hal-03630293v1>

Submitted on 4 Apr 2022

HAL is a multi-disciplinary open access archive for the deposit and dissemination of scientific research documents, whether they are published or not. The documents may come from teaching and research institutions in France or abroad, or from public or private research centers.

L'archive ouverte pluridisciplinaire **HAL**, est destinée au dépôt et à la diffusion de documents scientifiques de niveau recherche, publiés ou non, émanant des établissements d'enseignement et de recherche français ou étrangers, des laboratoires publics ou privés.



HAL Authorization

DOI: 10.1002/ ((please add manuscript number))

Article type: Full Paper

**Atomically Precise Prediction of 2D Self-Assembly of Weakly Bonded Nanostructures:
STM Insight into Concentration-Dependent Architectures**

*Mohamed El Garah, Arezoo Dianat, Andrea Cadeddu, Rafael Gutierrez, Marco Cecchini,
Timothy R. Cook, Artur Ciesielski,* Peter J. Stang,* Gianaurelio Cuniberti,* Paolo Samori**

Dr. M. El Garah, Dr. A. Cadeddu, Dr. M. Cecchini, Dr. A. Ciesielski, Prof. P. Samori
ISIS & icFRC, Université de Strasbourg & CNRS, 8 allée Gaspard Monge, 67000 Strasbourg,
France. E-mail: samori@unistra.fr, ciesielski@unistra.fr

Dr. A. Dianat, Dr. R. Gutierrez, Prof. G. Cuniberti
Faculty of Mechanical Science and Engineering, Institute for Materials Sciences and Max
Bergmann Center of Biomaterials, 01062 Dresden, Germany.
Institute for Materials Science, Dresden Center for Computational Materials Science
(DCCMS) and Max Bergmann Center of Biomaterials, Dresden University of Technology,
01062 Dresden, Germany. g.cuniberti@tu-dresden.de

Dr. T. R. Cook, Prof. P. J. Stang
Department of Chemistry, University of Utah, 315 South 1400 East, Salt Lake City, Utah
84112, United States. E-mail: stang@chem.utah.edu

Dr. T. R. Cook Current address: Department of Chemistry, University at Buffalo - SUNY,
Buffalo, New York 14260, United States

Keywords: ((self-assembly, hydrogen bonding, DFT, interfaces))

ABSTRACT

We report a joint experimental and computational study on the concentration-dependant self-assembly of a flat C_3 -symmetric molecule on a graphite surface. As a model system we have chosen a tripodal molecule, 1,3,5-tris(pyridin-3-ylethynyl)benzene, which can adopt either C_{3h} or C_s symmetry when planar, as a result of pyridyl rotation along the alkynyl spacers. DFT simulations of 2D nanopatterns at different surface coverage revealed that the molecule can generate different types of self-assembled motifs. We have analyzed the stability of fourteen 2D patterns and the influence of concentration. We found that ordered, densely packed monolayers and 2D porous networks are obtained at high and low concentrations, respectively. A concentration-dependent scanning tunnelling microscopy investigation of this molecular self-assembly system at a solution/graphite interface revealed four supramolecular motifs, which are in perfect agreement with those predicted by simulations. Therefore, our DFT method represents a key step forward toward the atomically precise prediction of molecular self-assembly on surfaces and at interfaces.

1. Introduction

The *ad hoc* design of molecular building blocks that undergo self-recognition processes constitutes a viable approach to form highly ordered two-dimensional architectures *via* self-assembly at surfaces and interfaces.^[1] Such supramolecular structures are of interest not only as a strategy for nanopatterning and surface templating, but also for more technologically high-end applications in sensing, nanoelectronics and nanophotonics.^[2] Among the various examples of supramolecular arrays on solid surfaces which have been reported to date,^[3] those featuring voids, so-called 2D porous networks, are of special importance.^[4] These periodic architectures that can be physisorbed on different substrates including metals^[5] and graphite,^[6] are attracting growing interest because they represent optimal motifs for studying the properties of molecules in confined spaces, thereby paving the way towards technological applications in nanoengineering and, more generally, in nanotechnology.^[7] A further distinct advantage of porous networks is their regular spatial arrangement of nanometer-sized cavities with uniform, well-defined shapes, that can be used for storage functionality or to control reactivities.^[8]

Theoretical simulations offer an alternative and complementary route to explore the self-assembly of molecular building blocks into 2D well-ordered supramolecular architectures on solid surfaces.^[9] Various approaches including methods based on all-atom molecular dynamics (MD),^[10] molecular mechanics (MM),^[11] density functional theory (DFT),^[12] and Monte Carlo (MC) simulations,^[13] have recently been developed to predict the 2D self-assembly and formation of supramolecular architectures on surfaces.

The molecular surface patterning at the solid/liquid interface is ruled by the interplay of molecule–molecule, molecule–solvent, solvent–substrate and molecule–substrate interactions, and is primarily driven by thermodynamic control.^[14] Therefore, the self-assembly of molecular building blocks can be steered *via* modification of external

macroscopic parameters including the type of solvent^[15] and/or the substrate used,^[16] temperature^[17] and solute concentration.^[12c, 13c, 14f, 18]

While the concentration-dependent self-assembly of monocomponent supramolecular architectures has been investigated in the past by scanning tunnelling microscopy (STM) at the solid/liquid interface, in particular by taking advantage of the reversible nature of multiple H-bonding^[18b] and van der Waals interactions between interdigitated alkyl chains,^[11, 14f] a recent example demonstrates that the self-assembly of weakly bonded pyridyl-containing molecules can be also tuned by varying the solute concentration.^[13c]

In this work we employ DFT calculations to effectively model and predict with atomic precision the concentration-dependent self-assembly of weakly interacting molecules adsorbed on a graphite surface. Computational results have been corroborated experimentally by STM imaging of the self-assembly at the solid/liquid interface. We focus our attention on 1,3,5-tris(pyridin-3-ylethynyl)benzene (**1**; **Figure 1a**), which consists of three pyridyl groups connected to a central benzene aryl ring through alkynyl moieties. Although, the self-assembly of a similar molecule, i.e. C_3 -symmetric 1,3,5-tris(pyridin-4-ylethynyl)benzene, has been recently reported by some of us^[13c] and other groups,^[19] in this work we address the complexity that arises when a building block can adopt multiple orientations: the pyridyl N atom located in the meta position offers an extremely rich self-assembly scenario. In particular, the relative directionality of the pyridyl groups can drastically influence the molecular self-assembly on solid substrates.

2. Results and discussion

2.1. MD simulations

Molecule **1** possesses three pyridyl rings connected to a central aryl ring through alkynyl moieties. Due to bond rotations, it can adopt C_{3h} or C_s symmetries when planar, with additional C_1 and C_{3v} orientations possible when out-of-plane pyridyl rings are considered

(Figure 1a,b). In order to quantify the population of the different regioisomers of **1**, and the probability of their existence at room temperature, a series of MD simulations were performed. Towards this end, 36 molecules of **1** were randomly deposited in vacuum and/or on a graphene slab. After thermal equilibration (10 ps, at room temperature and/or 80 °C) of the molecules, and Langevin dynamics (10 ns), regioisomers of **1** were identified (by analysing multiple snapshots). The probability of their existence was calculated using a Boltzmann distribution. Figure 1c shows that different regioisomers are favoured when the molecules are in vacuum versus physisorbed on graphene surface, which can be explained by considering the different rotational energy barriers in these two conditions. In vacuum, ~70% of the molecules adopt $1C_s$ (UUD) / $1C_s$ (DDU) conformations, with the remaining molecules identified as either $1C_1$ (URR) / $1C_1$ (RUU) (~4%), $1C_s$ (LRR) / $1C_s$ (RLL) (~10%), $1C_{3h}$ (RRR) / $1C_{3h}$ (LLL) (~10%) and $1C_s$ (LDR) / $1C_s$ (RUL) (~4%). It is noteworthy that such a probability distribution was not affected by the increasing the temperature during MD. P(x) analysis of the simulations performed in the presence of a graphene surface revealed that only two species, namely C_{3h} (RRR) / C_{3h} (LLL) (~25%) and C_s (LRR) / C_s (RLL) (~75%) are favoured in simulations performed at RT and 80 °C. Because of the non-planar nature of the other regioisomers, and their low adsorption energies, the probability of their existences on graphene surfaces is close to zero.

3.2. Theoretical Studies

Based on previous studies of weakly interacting tripodal molecules physisorbed on solid surfaces,^[13c, 14f, 18a] we have simulated several potential 2D self-assembled structures based on **1**. These nanopatterns differ in their molecular densities, as well as in their relative orientations of molecules, which can be physisorbed in parallel (P) or antiparallel (A) fashions. Moreover, as revealed by MD simulations, molecule **1**, can adopt either C_{3h} (RRR) / C_{3h} (LLL) or C_s (LRR) / C_s (RLL) symmetries, as a result of pyridyl rotation along the alkynyl

spacer. Consequently, fourteen 2D structures were investigated by means of DFT. **Figure 2** shows seven C_{3h} (LLL) (red) and C_s (LRR) (blue) based architectures, and includes densely packed 1A1 and 1P1 structures, and five porous networks, i.e. 1A2-1A5 and 1P2. Notably, the C_{3h} (RRR) vs. C_{3h} (LLL) isomers, as well as C_s (LRR) vs. C_s (RLL), are mirror representations of the same architectures; therefore, hereafter the conformation of C_{3h} and C_s regioisomers (e.g. RRR) will be omitted for the sake of clarity.

To get an in-depth understanding on the stabilization energies of the simulated structures, three parameters were investigated: (i) the area of the surface (graphite) occupied by a single molecule **1** (A_{mol}), (ii) the energy of intermolecular interactions (E_{int}), and (iii) the adsorption energy (E_{ads}).

Firstly, for each crystalline pattern obtained from simulations of the unit cell parameters, i.e., the length of the vectors a and b , the angle between the vectors (α), the unit cell area (A), the number of molecules in the unit cell (N_{mol}) and the area occupied by a single molecule in the unit cell (A_{mol} , with $A_{mol} = A/N_{mol}$) have been extracted and summarized in Table 1. A careful analysis of the unit cell parameters revealed that A varies from 3.2 to 5.5 nm² corresponding to A1 and P2 architectures, respectively.

Furthermore, the unit cell of each self-assembled structure contains two molecules of **1**, therefore proportional changes in A_{mol} can be observed. While the symmetry of **1** did not affect either A nor A_{mol} , remarkable differences in both E_{int} and E_{ads} normalized per unit area, have been monitored between the patterns based on the C_{3h} and C_s regioisomers of **1**. **Figure 3a** reveals that in the case of all investigated 2D patterns, the E_{ads} per unit area is one order of magnitude greater than E_{int} , which proves that the self-assembly of **1** on graphite surfaces is mainly driven by molecular physisorption rather than E_{int} . Furthermore, a gradual decrease of both E_{ads} and E_{int} has been observed with decreasing molecular densities on the graphene surface. Figure 3b displays the effect of the symmetry of **1** on the total formation energy of the 2D nanopatterns ($E_{tot} = E_{ads} + E_{int}$). Remarkably, the majority of the self-assembled

architectures are expected to be formed *via* self-association of the C_s regioisomers of **1**, as their E_{tot} is notably lower than the C_{3h} analogues, although for A4, A5 and P2 structures E_{tot} was found to be marginally lower than that of the C_{3h} ones. This can be explained by considering both the nature and density of the intermolecular interactions involved in the stabilization of the investigated nanopatterns. Within 2D patterns, several intermolecular forces play an important role during self-assembly of **1**. These can be divided into two classes: *i*) attractive (pyridyl)N \cdots H–C(pyridyl/aryl) and van der Waals interactions between **1**; *ii*) repulsive (pyridyl)N \cdots N(pyridyl) and (pyridyl/aryl)C–H \cdots H–C(pyridyl/aryl) electrostatic repulsions. Furthermore, we have investigated the possible dipolar interaction between pyridyl rings of neighboring molecules, which if strong enough, could dominate the intermolecular interactions. We have calculated the dipole moments of molecular species in their C_{3h} and C_s symmetries using the VASP *ab initio* code based on density functional theory. The computed dipole moments amounted to 3.54 and 0.35 Debye for C_{3h} for C_s , respectively. As a result of the molecular ordering in the self-assembled monolayers the molecular dipole moments are all arranged parallel within the unit cell, we have therefore used a simple expression to estimate the contribution arising from the dipole-dipole interactions: $E_{dip-dip} = 2(\mu_1\mu_2/4\pi\epsilon_0)r^{-3}$. In the case of the larger dipole moment 3.54 D, i.e. in the case of molecules adopting C_{3h} conformation, and for a typical intermolecular separation of ~ 3.6 Å, the dipolar interaction energy (normalized by the unit cell area) was found as small as 0.06 eV/nm². If compared with the intermolecular hydrogen bonding energies shown in Figure 2a, it appears clearly that latter are roughly three orders of magnitude larger than dipolar interaction energies. Despite its relatively weak interaction energy, the (pyridyl)N \cdots H–C(pyridyl/aryl) H-bonding motif has been used by us, and other groups to drive the formation of 2D supramolecular structures on solid inert surfaces.^[13c, 20] The results presented above suggest that, depending of the molecular density on the graphite substrate, molecule **1** can generate a

variety of self-assembly motifs. To validate this, concentration dependent STM experiments were performed.

3.3. STM investigation

STM was used to explore the self-assembly behaviour of molecule **1** when physisorbed at a solution/graphite interface. Initially, we investigated the self-assembled structures by applying a drop of a 1 mM solution of **1** in 1-phenyloctane on a graphite surface. **Figures 4a,b** show height STM images (i.e., recorded in constant-current mode) of the obtained physisorbed monolayer. It displays a polycrystalline structure consisting of crystalline domains of hundreds of square nanometres in size. These domains were found to be stable on the surface for 3-4 hours. For each crystalline pattern obtained from molecule **1** self-assembled on HOPG, the unit cell parameters, i.e., the length of the vectors a and b , angle between the vectors (α), unit cell area (A), number of molecules in the unit cell (N_{mol}) and area occupied by a single molecule in the unit cell (A_{mol}) are given in **Table 2**. The latter parameter has been compared with theoretical data (Th. A_{mol}), which allows for precise pattern assignment. The formation of such a densely packed 2D structure of **1** shown in Figure 4a,b is in agreement with the computed A1 motif, in which the molecules self-assemble in antiparallel fashion. Moreover, as revealed by DFT simulations the molecules of **1** adopt C_s symmetry, therefore the 2D nanopattern can be described as $1C_sA1$, which is energetically more favored than $1C_{3h}A1$. The supramolecular motif is stabilized by strong molecule–graphite van der Waals interactions and molecule–molecule van der Waals and electrostatic interactions. The latter may arise from the formation of weak $N(\text{pyridyl})\cdots H-C(\text{aryl})$ H-bonds between adjacent molecules.^[13c]

As revealed by DFT simulations, the formation of self-assembled motifs of **1** strongly depends on the molecular surface density, i.e. the number of molecules per surface area, which can be experimentally varied by changing the concentration of the solution of **1** and

potentially leads to the generation of different supramolecular motifs; because of this, we extended our experimental studies to films prepared from dilute solutions, by lowering the concentration 0.05 mM for each trial. STM imaging of the monolayers prepared from the solutions ranging from 1 ± 0.01 mM down to 0.65 ± 0.01 mM, revealed the existence of **1A1** architectures, exclusively. Notably, these results have been obtained using an A scanner (Veeco), therefore encompassing a maximum area of 1×1 μm . The generation of 2D crystalline domains featuring different self-assembly motifs (see unit cell parameters in Table 2), was achieved by applying a drop of 0.60 ± 0.01 mM (down to 0.40 ± 0.01 mM) solution on HOPG surface (Figs. 4d, e). In contrast to the monolayers prepared from concentrated solutions, the molecules were found to self-assemble in parallel fashion. Noteworthy, the difference in the STM imaging contrast between different areas of the STM image is the result of the Moirè effect, i.e. the electronic mismatch/interference of the supramolecular lattice and the underlying HOPG surface. By linking the experimental results, in particular the area occupied by a single molecule **1**, with our theoretical calculations, we conclude that the supramolecular ensemble can be well described by the formation of a **1C_{3h}P1** structure (see model in Fig. 4f).

STM analysis of films prepared from more dilute solutions, i.e. concentrations ranging from 0.35 ± 0.01 mM down to 0.20 ± 0.01 mM, revealed the formation of 2D porous crystalline domains (Figure 4g,h). These porous structures can be described by the formation of dimer-like subunits (marked in blue in Figure 4i), which further expand into lamellar arrays (marked in green in Figure 4i). Furthermore, as a consequence of the electrostatic interactions between the pyridyl groups of neighbouring lamellas, a porous **1A5** 2D supramolecular structure was formed.

As revealed by DFT simulations, more loosely packed nanopatterns of **1** can be formed at lower concentrations; in light of this finding we have extended our experimental studies to films prepared from highly dilute (0.15 ± 0.05 mM) solutions. STM imaging of these films

(Figure 4j,k) provided evidence for the generation of 2D porous crystalline domains markedly different than that of 1A5. The unit cell parameters (Table 1) lead to $A_{mol} = (5.3 \pm 0.1) \text{ nm}^2$, which corresponds to a 1P2 architecture. Although the 1C_sA1 and 1C_sP1 structures were found to be energetically more favourable than 1C_{3h}A1 and 1C_{3h}P1 by 0.33 eV nm⁻² and 0.18 eV nm⁻², respectively, the E_{tot} difference between 1C_sA5 and 1C_{3h}A5 (0.06 eV nm⁻²), as well as 1C_sP2 and 1C_{3h}P2 (0.04 eV nm⁻²) is minimal. Therefore, we decided to not assign any symmetry groups to the 1A5 and 1P2 architectures.

As shown by DFT simulations, the average E_{tot} in defect-free layers of 1A5 (-1.32 eV nm⁻²) and 1P2 (-1.22 eV nm⁻²) porous networks are much higher than those in the 1A2, 1A3 and 1A4 assemblies (-2.27, -1.96 and -1.51 eV nm⁻², respectively), therefore the existence of the latter at the solid/liquid interface should be also monitored. Numerous additional experiments were carried out using solutions with concentrations spanning from 1.00 to 0.05 mM in order to study the potential coexistence of 1A1, 1P1, 1A5 and 1P2 architectures, as well as formation of other possible nanopatterns. Yet, only one type of 2D structure was exclusively observed.

3. Conclusion

In summary, we have demonstrated that complex 2D supramolecular architectures on solid surfaces can be effectively simulated using DFT and directly compared to STM imaging at the solid/liquid interface in order to ultimately unravel with an atomic precision the molecular self-assembly in 2D. As revealed by DFT simulations, the formation of self-assembled motifs of **1** strongly depends on the molecular surface density, i.e. the number of molecules per surface area. We have shown experimentally by STM imaging at the solid/liquid interface that the self-assembly behaviour of **1** on graphite is concentration dependent, forming architectures characterized by different molecular surface density and self-assembly motifs, i.e. either densely packed 1A1 and 1P1 arrays or 2D porous 1A5 and 1P2 structures at high or

low concentrations, respectively. The choice of a molecular building block undergoing weak H-bonding was demonstrated being key in order to operate under full thermodynamic control, thereby avoiding polymorphisms at a given concentration (or surface coverage) as a result of an efficient self-healing behaviour of the self-assembled structures. The ability to predict the molecular surface density regimes for which a given supramolecular array will be created on a given substrate is extremely beneficial when targeting a particular architecture, obviating the need for material-intensive experimental trials at countless concentration regimes.

4. Experimental Section

Synthesis: Building block **1** was formed through Sonogashira couplings as reported in the literature.^[21]

Molecular dynamics: All force-field calculations were performed with the program CHARMM^[22] using the implementation in the c35b1 update. Parameterization of the pyridyl building blocks was done through the Merck molecular force field MMFF94^[23] automatic module implemented in CHARMM. A graphene C-atom slab embedded in an orthorhombic box with periodic boundary conditions (PBCs) was used to represent the STM substrate. The MM model for graphene has been presented elsewhere.^[24]

Density functional theory: Density functional calculations were performed within a combined plane-wave and atomic-orbital approach as implemented in the cp2k code (www.cp2k.org). The PBE plane wave functional and the DZVP (double zeta for valence electrons plus polarization function) localized basis sets were used for geometry optimizations. Dispersion corrections were taken into account by the Grimme parametrization.^[25] After geometry optimization, single point energy calculations with the hybrid B3LYP/6-31G(d,p) functional were carried out. In the first step, each self-assembled 2D nanopattern, the dimer configurations of **1** (see Figure 1) in its C_{3h} and C_s -symmetry were first relaxed with periodic boundary conditions in the absence of the graphene substrate. The intermolecular distances

were varied and the cell lattice parameters adjusted accordingly in order to obtain the energetically most favourable configurations. In a subsequent step, the lattice vectors of the graphene substrate were adjusted to the corresponding molecular network lattice parameters. To avoid non-physical artifacts related to the incommensurability between graphite lattice constant and the lattice constant of the unit cell of the molecular assembly, graphite lattice constant has been matched to that of a given molecular assembly. Otherwise, the lattice parameters of the assembly could be strongly modified by the mismatch upon subsequent relaxation of the whole structure. This unit cell adjustment was necessary for avoiding artifacts related to the incommensurability between the in-plane graphite lattice constant and the lattice constant of the unit cell of the molecular assembly. This led to a slight stretching of graphite of about 3% for some network configurations, causing a slight reduction of the adsorption energy between the molecules and the substrate due to broadening of π -orbitals. This two-step approach is justified, since the H-bonding within the molecular network is the relevant interaction determining the network stability. The corresponding adsorption energies of the different molecular arrangements were defined as described in Eq. 1:

$$E_{ads} = E_{dimer/graphene} - E_{graphene} - E_{dimer} \quad (1)$$

where $E_{dimer/graphene}$, $E_{graphene}$ and E_{dimer} (C_{3h} or C_s) are the total energies of the dimer of **1** adsorbed on graphene, of isolated graphene and of the isolated dimer, respectively. Different configurations of dimer of **1** have been shown in Figure S1 in Supplementary Information. The average equilibrium distance of the molecules to the graphene surface is ca. 3.4 ± 0.1 Å depending on the network structure.

The inter-molecular interaction energy E_{int} of the suggested theoretical assembly models was computed as

$$E_{int} = E_{SAM} - nE_1 \quad (1)$$

where E_{SAM} is the total energy of a supercell containing only the molecular assembly, i.e. without the graphite substrate, and n is the number of molecules **1** with energy E_1 , within a given self-assembly motif.

Scanning Tunnelling Microscopy: STM measurements were performed using a Veeco scanning tunnelling microscope (multimode Nanoscope III, Veeco) at the interface between a highly oriented pyrolytic graphite (HOPG) substrate and a supernatant solution, thereby mapping a maximum area of $1 \times 1 \mu\text{m}$. Solution of molecules was applied to the basal plane of the surface. For STM measurements, the substrates were glued to a magnetic disk and an electric contact was made with silver paint (Aldrich Chemicals). The STM tips were mechanically cut from a Pt/Ir wire (90/10, diameter 0.25 mm). The raw STM data were processed through the application of background flattening and the drift was corrected using the underlying graphite lattice as a reference. The lattice was visualized by lowering the bias voltage to 20 mV and raising the current up to 65 pA. A solution was made by dissolving **1** in chloroform and diluting with 1-phenyloctane to give the concentrations described in the section below. STM imaging was carried out in constant height mode without turning off the feedback loop to avoid tip crashes. Monolayer pattern formation was achieved by applying 4 μL of solution onto freshly cleaved HOPG. The STM images were recorded at room temperature once a negligible thermal drift was achieved. All of the molecular models were minimized with DFT (see section above) and processed with QuteMol visualization software (<http://qutemol.sourceforge.net>).

Supporting Information ((delete if not applicable))

Supporting Information is available from the Wiley Online Library or from the author.

Acknowledgements

We thank Nicolas Merstorf for performing preliminary calculations on molecule **1**. This work was financially supported by the ERC project SUPRAFUNCTION (GA-257305), the Agence Nationale de la Recherche through the LabEx project Chemistry of Complex Systems (ANR-10-LABX-0026_CSC), and the International Center for Frontier Research in Chemistry (icFRC). We acknowledge support by the German Research Foundation (DFG) within the

Cluster of Excellence "Center for Advancing Electronics Dresden" and by the Center for Information Services and High Performance Computing (ZIH) at TU Dresden for computational resources. PJS thanks the NSF (CHE 0820955) for financial support.

Received: ((will be filled in by the editorial staff))

Revised: ((will be filled in by the editorial staff))

Published online: ((will be filled in by the editorial staff))

- [1] A. Langner, S. L. Tait, N. Lin, C. Rajadurai, M. Ruben, K. Kern, *Proc. Natl. Acad. Sci. U.S.A.* **2007**, *104*, 17927.
- [2] D. Bonifazi, S. Mohnani, A. Llanes-Pallas, *Chem. Eur. J.* **2009**, *15*, 7004.
- [3] a) S. De Feyter, F. C. De Schryver, *Chem. Soc. Rev.* **2003**, *32*, 139; b) E. Gomar-Nadal, M. M. S. Abdel-Mottaleb, S. De Feyter, J. Veciana, C. Rovira, D. B. Amabilino, F. C. De Schryver, *Chem. Commun.* **2003**, 906; c) A. M. Jackson, J. W. Myerson, F. Stellacci, *Nat Mater* **2004**, *3*, 330; d) S. S. Li, H. J. Yan, L. J. Wan, H. B. Yang, B. H. Northrop, P. J. Stang, *J. Am. Chem. Soc.* **2007**, *129*, 9268; e) J. M. MacLeod, O. Ivasenko, D. F. Perepichka, F. Rosei, *Nanotechnology* **2007**, *18*, 3347; f) A. Centrone, E. Penzo, M. Sharma, J. W. Myerson, A. M. Jackson, N. Marzari, F. Stellacci, *P Natl Acad Sci USA* **2008**, *105*, 9886; g) S. Lei, J. Puigmarti-Luis, A. Minoia, M. Van der Auweraer, C. Rovira, R. Lazzaroni, D. B. Amabilino, S. De Feyter, *Chem. Commun.* **2008**, 703; h) S. B. Lei, K. Tahara, K. Müllen, P. Szabelski, Y. Tobe, S. De Feyter, *ACS Nano* **2011**, *5*, 4145; i) S. Mohnani, D. Bonifazi, *Coordin Chem Rev* **2010**, *254*, 2342; j) R. Chakrabarty, P. S. Mukherjee, P. J. Stang, *Chem Rev* **2011**, *111*, 6810.
- [4] a) L. J. Wan, *Acc. Chem. Res.* **2006**, *39*, 334; b) F. Cicoira, C. Santato, F. Rosei, in *Top. Curr. Chem.*, Springer, **2008**, 203; c) H. Liang, Y. He, Y. C. Ye, X. G. Xu, F. Cheng, W. Sun, X. Shao, Y. F. Wang, J. L. Li, K. Wu, *Coordin Chem Rev* **2009**, *253*, 2959.
- [5] a) J. V. Barth, *Annu Rev Phys Chem* **2007**, *58*, 375; b) A. Kühnle, *Curr. Opin. Colloid Interface Sci.* **2009**, *14*, 157.
- [6] a) N. Katsonis, E. Lacaze, B. L. Feringa, *J. Mat. Chem.* **2008**, *18*, 2065; b) T. Kudernac, S. B. Lei, J. A. A. W. Elemans, S. De Feyter, *Chem. Soc. Rev.* **2009**, *38*, 402.

- [7] J. V. Barth, G. Costantini, K. Kern, *Nature* **2005**, *437*, 671.
- [8] L. Piot, D. Bonifazi, P. Samorì, *Adv Funct Mater* **2007**, *17*, 3689.
- [9] C. A. Palma, M. Cecchini, P. Samorì, *Chem. Soc. Rev.* **2012**, *41*, 3713.
- [10] a) M. Linares, A. Minoia, P. Brocorens, D. Beljonne, R. Lazzaroni, *Chem. Soc. Rev.* **2009**, *38*, 806; b) C. A. Palma, P. Samorì, M. Cecchini, *J. Am. Chem. Soc.* **2010**, *132*, 17880; c) A. Ciesielski, A. Cadeddu, C. A. Palma, A. Gorczynski, V. Patroniak, M. Cecchini, P. Samorì, *Nanoscale* **2011**, *3*, 4125.
- [11] B. A. Hermann, C. Rohr, M. B. Gamba, A. Malecki, M. S. Malarek, E. Frey, T. Franosch, *Phys. Rev. B* **2010**, *82*, 165451.
- [12] a) N. Lin, S. Stepanow, M. Ruben, J. V. Barth, *Top. Curr. Chem.* **2009**, *287*, 1; b) X.-J. Ma, Y.-L. Yang, K. Deng, Q.-D. Zeng, C. Wang, K.-Q. Zhao, P. Hu, B.-Q. Wang, *ChemPhysChem* **2007**, *8*, 2615; c) A. Ciesielski, A. R. Stefankiewicz, F. Hanke, M. Persson, J.-M. Lehn, P. Samorì, *Small* **2011**, *7*, 342.
- [13] a) P. Szabelski, S. De Feyter, M. Drach, S. B. Lei, *Langmuir* **2010**, *26*, 9506; b) P. Szabelski, S. De Feyter, *CrystEngComm* **2011**, *13*, 5542; c) A. Ciesielski, P. J. Szabelski, W. Rzyško, A. Cadeddu, T. R. Cook, P. J. Stang, P. Samorì, *J. Am. Chem. Soc.* **2013**, *135*, 6942.
- [14] a) S. Ahn, A. J. Matzger, *J. Am. Chem. Soc.* **2010**, *132*, 11364; b) A. Ciesielski, C.-A. Palma, M. Bonini, P. Samorì, *Adv Mater* **2010**, *22*, 3506; c) A. Ciesielski, P. Samorì, *Nanoscale* **2011**, *3*, 1397; d) S. De Feyter, A. Gesquiere, M. M. Abdel-Mottaleb, P. C. M. Grim, F. C. De Schryver, C. Meiners, M. Sieffert, S. Valiyaveetil, K. Müllen, *Acc. Chem. Res.* **2000**, *33*, 520; e) J. F. Dienstmaier, K. Mahata, H. Walch, W. M. Heckl, M. Schmittel, M. Lackinger, *Langmuir* **2010**, *26*, 10708; f) S. B. Lei, K. Tahara, F. C. De Schryver, M. Van der Auweraer, Y. Tobe, S. De Feyter, *Angew. Chem. Int. Ed.* **2008**, *47*, 2964; g) R. Gutzler, T. Sirtl, J. F. Dienstmaier, K. Mahata, W. M. Heckl, M. Schmittel, M. Lackinger, *J. Am. Chem. Soc.* **2010**, *132*, 5084.

- [15] L. Kampschulte, M. Lackinger, A. K. Maier, R. S. K. Kishore, S. Griessl, M. Schmittel, W. M. Heckl, *J. Phys. Chem. B* **2006**, *110*, 10829.
- [16] T. Kudernac, N. Sandig, T. F. Landaluce, B. J. van Wees, P. Rudolf, N. Katsonis, F. Zerbetto, B. L. Feringa, *J. Am. Chem. Soc.* **2009**, *131*, 15655.
- [17] M. O. Blunt, J. Adisojoso, K. Tahara, K. Katayama, M. Van der Auweraer, Y. Tobe, S. De Feyter, *J. Am. Chem. Soc.* **2013**, *135*, 12068.
- [18] a) K. Tahara, S. Okuhata, J. Adisojoso, S. B. Lei, T. Fujita, S. De Feyter, Y. Tobe, *J. Am. Chem. Soc.* **2009**, *131*, 17583; b) L. Kampschulte, T. L. Werblowsky, R. S. K. Kishore, M. Schmittel, W. M. Heckl, M. Lackinger, *J. Am. Chem. Soc.* **2008**, *130*, 8502; c) K. S. Mali, J. Adisojoso, E. Ghijsens, I. De Cat, S. De Feyter, *Acc. Chem. Res.* **2012**, *45*, 1309.
- [19] a) S. Vijayaraghavan, D. Ecija, W. Auwarter, S. Joshi, K. Seufert, M. Drach, D. Nieckarz, P. Szabelski, C. Aurisicchio, D. Bonifazi, J. V. Barth, *Chem. Eur. J.* **2013**, *19*, 14143; b) D. Ecija, S. Vijayaraghavan, W. Auwärter, S. Joshi, K. Seufert, C. Aurisicchio, D. Bonifazi, J. V. Barth, *ACS Nano* **2012**, *6*, 4258.
- [20] a) U. Ziener, J.-M. Lehn, A. Mourran, M. Möller, *Chem. Eur. J.* **2002**, *8*, 951; b) L. Kampschulte, S. Griessl, W. M. Heckl, M. Lackinger, *J. Phys. Chem. B* **2005**, *109*, 14074; c) J. Zhang, B. Li, X. F. Cui, B. Wang, J. L. Yang, J. G. Hou, *J. Am. Chem. Soc.* **2009**, *131*, 5885.
- [21] B. Brusilowskij, S. Neubacher, C. A. Schalley, *Chem. Commun.* **2009**, 785.
- [22] B. R. Brooks, W. Yang, D. M. York, M. Karplus, *J. Comput. Chem.* **2009**, *30*, 1545.
- [23] T. A. Halgren, *J. Comput. Chem.* **1996**, *17*, 490.
- [24] J. Björk, F. Hanke, C. A. Palma, P. Samorì, M. Cecchini, M. Persson, *J. Phys. Chem. Lett.* **2010**, *1*, 3407.
- [25] S. Grimme, *J. Comp. Chem.* **2006**, *27*, 1787.

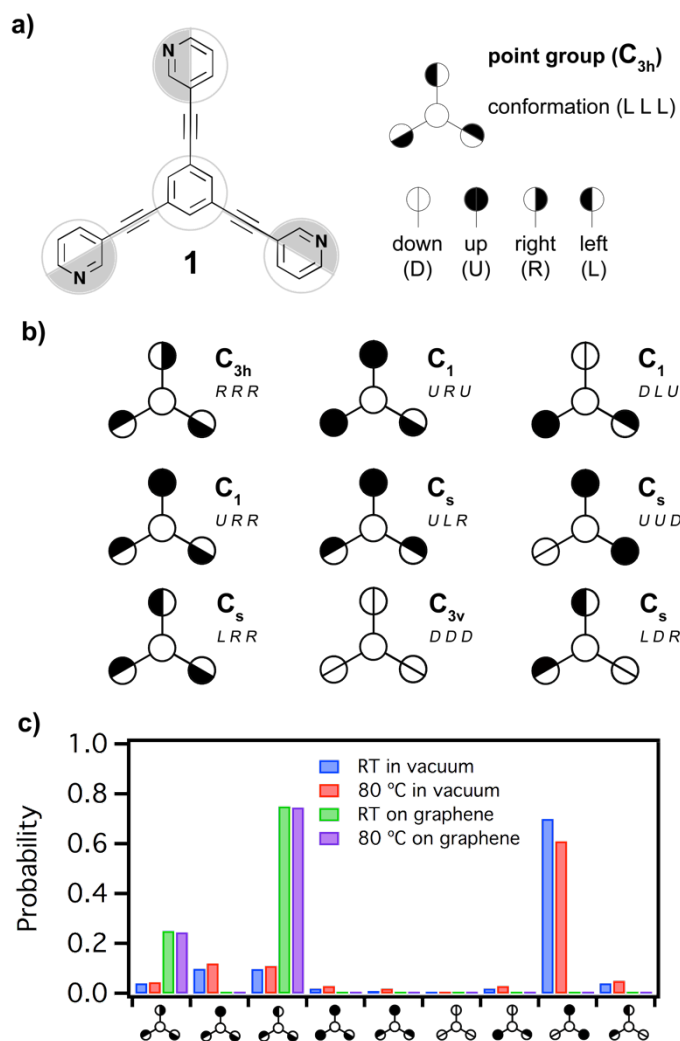


Figure 1. a) Chemical structure of 1,3,5-tris(pyridin-3-ylethynyl)benzene (**1**); b) Exploratory scheme of the symbols used to describe different relative geometries of **1**. The position of each pyridyl ring relative to the core is represented with an half-filled or fully filled circles indicating whether the rings are coplanar (half-filled), or oriented orthogonally, with the pyridyl nitrogen pointing up (fully filled black) or down (fully filled white). Point group symmetry and conformation (R = right, U = up, L = left, D = down) of **1** regioisomers used in the MD and DFT calculations; (c) Probability of **1** to exist according to different configurations in vacuum and on the graphene slab, computed using Boltzmann distribution.

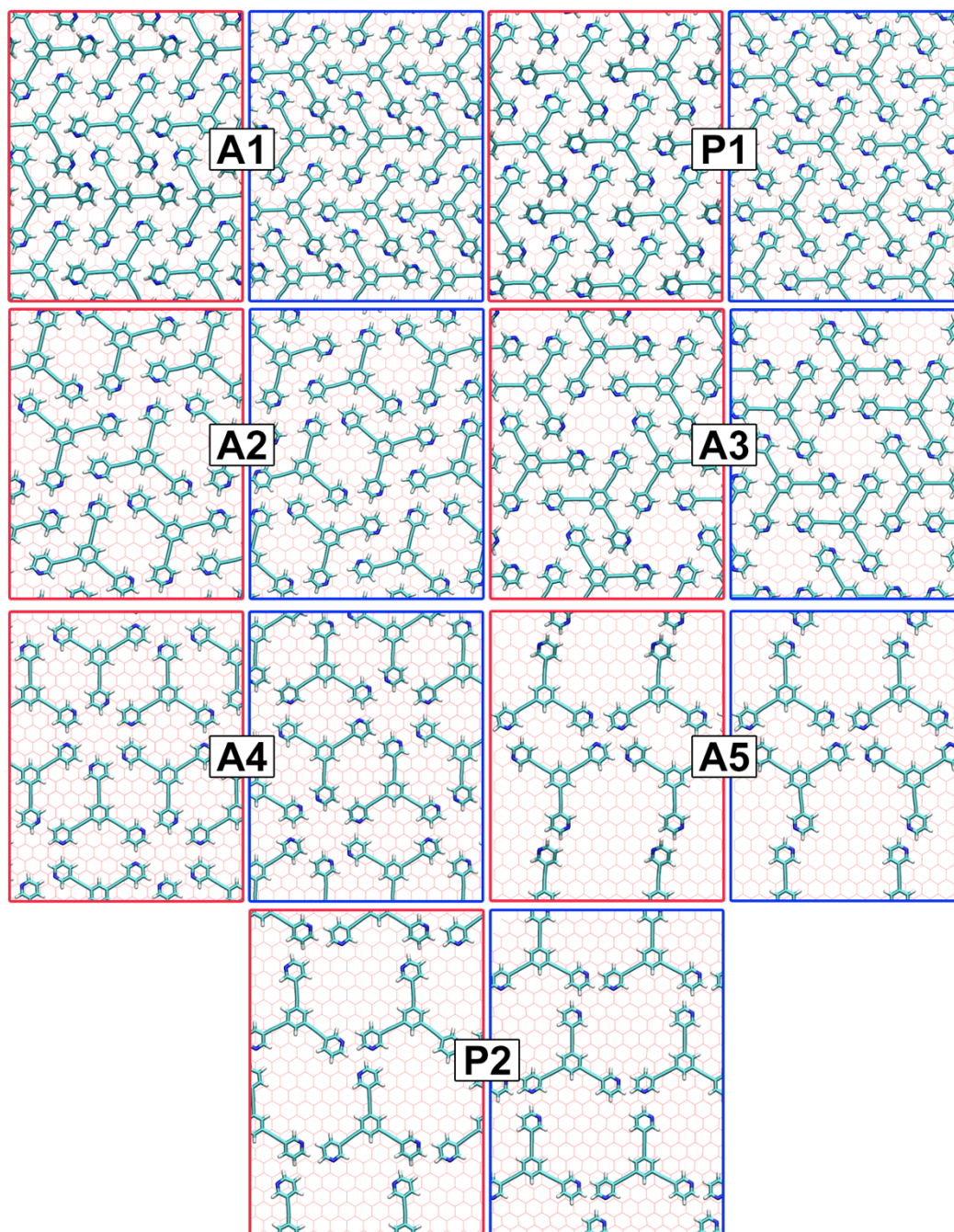


Figure 2. Simulated 2D supramolecular architectures of **1** adsorbed on a graphene surface. The letter codes correspond to the relative parallel (P) and antiparallel (A) orientations of the molecules. The frame colours correspond to different symmetries adopted by **1**: C_{3h} (red) and C_s (blue).

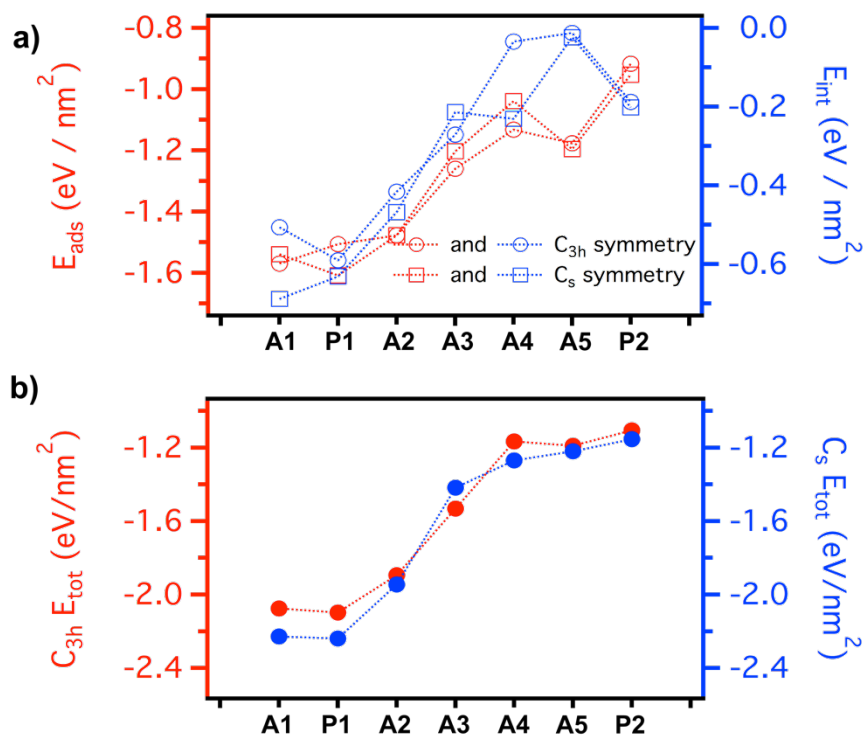


Figure 3. (a) Calculated adsorption (E_{ads} , in red) and intermolecular interaction (E_{int} , in blue) energies per unit area of different 2D nanopatterns formed by C_{3h} (circles) and C_s (squares) regioisomers of **1**. (b) Comparison of the total formation energy ($E_{tot} = E_{ads} + E_{int}$) of C_{3h} (in red) and C_s (in blue) based self-assembled structures.

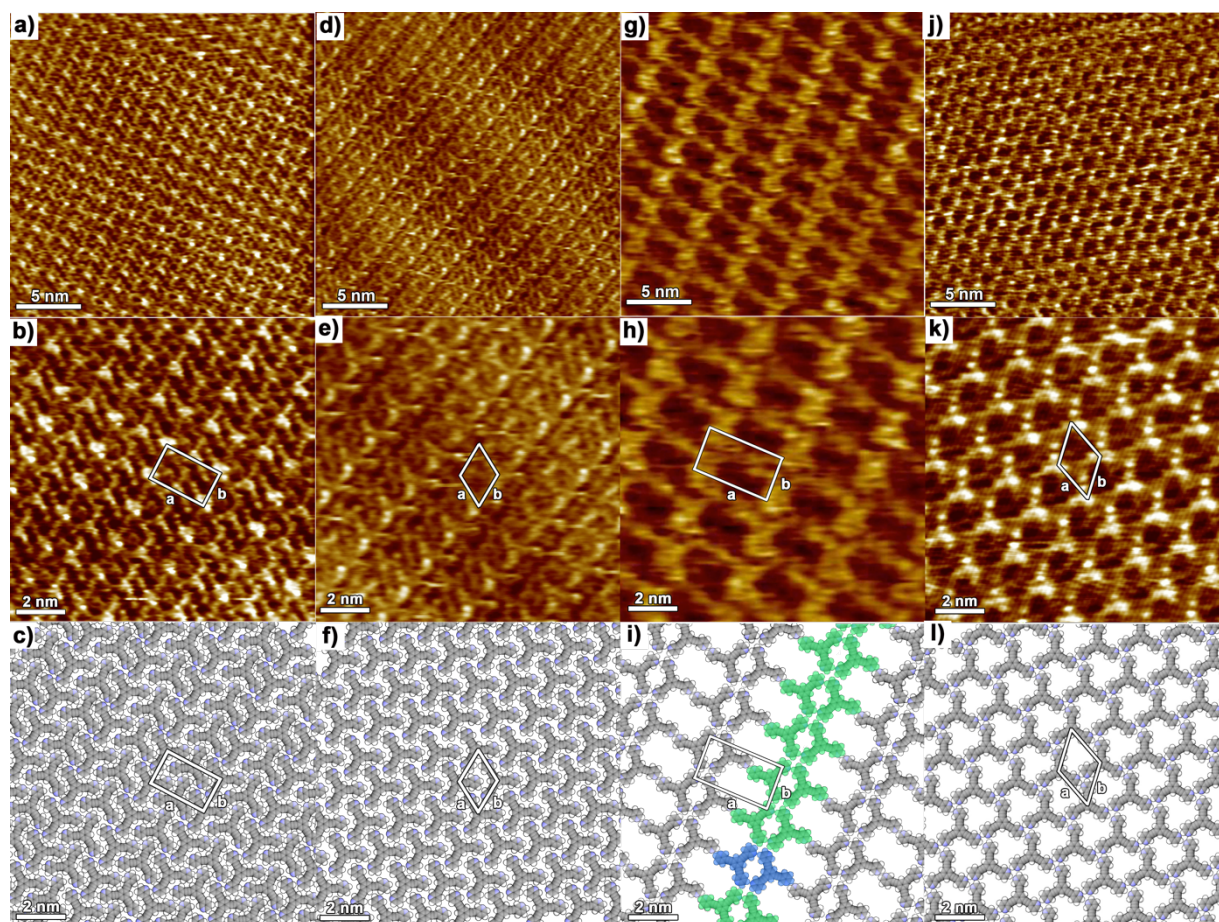


Figure 4. STM height images and proposed molecular packing motifs of supramolecular structures of **1** self-assembled at the solid/liquid interface from a solution of **1** in 1-phenyloctane at different concentration (c): $c = 1 - 0.65$ mM - **1A1** (a-c), $c = 0.60 - 0.40$ mM - **1P1** (d-f), $c = 0.35 - 0.20$ mM - **1A5** (g-i) and $c = 0.15 - 0.05$ mM - **1P2** (j-l). Tunnelling parameters: average tunnelling current (I_t) = 25-30 pA, tip bias voltage (V_t) = 400-550 mV.

Table 1. Unit cell parameters of the self-assembled structures of **1** investigated by DFT

Structure	a [nm]	b [nm]	α [°]	A [nm ²]	N_{mol}	A_{mol} [nm ²]
1A1	2.56	1.24	90	3.17	2	1.58
1P1	2.70	1.24	90	3.35	2	1.67
1A2	2.00	2.00	60	3.46	2	1.73
1A3	2.45	1.70	90	4.16	2	2.08
1A4	2.20	2.20	60	4.19	2	2.09
1A5	3.10	1.72	90	5.33	2	2.66
1P2	1.85	1.71	60	2.74	1	2.74

Table 2. Unit cell parameters of the structure **1A1**, **1P1**, **1A5** and **1P2** compared with theoretically predicted values.

Concentration range [mM]	Structure	<i>a</i> [nm]	<i>b</i> [nm]	<i>α</i> [°]	<i>A</i> [nm ²]	<i>N_{mol}</i>	<i>A_{mol}</i> [nm ²]	Th. <i>A_{mol}</i> [nm ²]
1 - 0.65 mM	1A1	2.5 ± 0.1	1.3 ± 0.1	90 ± 2	3.3±0.2	2	1.6±0.1	1.6
0.60 - 0.40 mM	1P1	1.4 ± 0.1	1.4 ± 0.1	60 ± 2	1.7±0.1	1	1.7±0.1	1.7
0.35 - 0.20 mM	1A5	3.0 ± 0.1	1.8 ± 0.1	90 ± 2	5.4±0.1	2	2.7±0.1	2.6
0.15 - 0.05 mM	1P2	1.8 ± 0.1	1.8 ± 0.1	60 ± 2	2.8±0.1	1	2.8±0.1	2.7